Simultaneous Wireless Power and Multibit Signals Transfer System With Hybrid Modulation Waves PWM Control

Chenyang Xia, *Member, IEEE*, Hongtai Zhang, Nan Wei, Shuze Zhao, Jiaan Yan, Xiangyu Song, Lijuan Xiang, and Zhijuan Liao

***Abstract*—The existing simultaneous wireless power (SWP) and information transfer can only achieve serial signal transmission and it is hard to decouple the power and signal transmission without the additional circuits. To solve these problems, a SWP and multibit signals transfer technology is proposed in this article. Based on the working principle of the hybrid modulation waves pulsewidth modulation control technology, the power and multibit signals are modulated into the system through the modulation waves with different frequencies. Therefore, the signal transmission no longer depends on the power transmission, and the signal transmission rate is multiplied through the realization of parallel signals transmission. Subsequently, the parameter selection criterion of the signal channel is given by analyzing the signal transmission rate and the interference between the power and signal transmission. Finally, the proposed technology is verified with experimental results. The experimental results demonstrate that the power and two-bit signals can be transmitted stably. Compared to the serial transmission, the band signal transmission rate is increased by two times.**

***Index Terms*—Hybrid modulation wave, multibit signals, pulsewidth modulation (PWM) control, simultaneous wireless power and information transfer.**

I. Introduction

THE wireless power transfer (WPT) technology has effectively improved the safety and flexibility of electricity transfer due to the complete isolation between the power supply and the electrical equipment, which is widely used in medical instruments [1], [2], rail transportation [3], and electric vehicles [4].

With the expanding demands for WPT technology applications, stable communication between the primary coil and the secondary coil is essential. Simultaneous wireless power and information transfer (SWPIT) technology has obtained more attention.

The existing SWPIT systems can be mainly classified into modules communication [5], [6], dual-channel transmission [7]–[9], and single-channel transmission [10]–[24]. Modules communication technology uses wireless modules to transmit signals. The wireless modules include the radio-frequency module, Wi-Fi, and so on, which is the common method used for wireless communication, however, the communication modules are costly and less stable in the high power rated WPT system. The dual-channel transmission technology needs to add an extra coil for the signal transmission. Therefore, the dual-channel transmission technology is not suitable for practical applications with narrow spaces such as implantable medical equipment. The additional coil will also increase the system cost. Compared with the dual-channel transmission technology and modules communication technology, the single-channel transmission technology can not only eliminate the additional coil and expensive communication modules but also increase the flexibility of the WPT system.

For single-channel simultaneous power and signal transmission technology, there are mainly three methods: energy envelope modulation [10]–[13], signal carrier wave injection [14]–[19], and harmonic utilization [20]–[23].

For the energy envelope modulated SWPIT technology, the signal is directly modulated on the power carrier through amplitude-shift keying (ASK), frequency-shift keying (FSK), and phase-shift keying (PSK) technology. The modulated method uses the same carrier for the power and signal transmission. In [10] and [11], the methods using the drain bias of a class E power amplifier and the dynamic bias of a positive channel metal oxide semiconductor are proposed to perform ASK modulation. The transistor modulates the signal characteristics onto the energy envelope. In [12], the PSK technology is applied to modulate the phase difference between the rectifier input voltage and the receiver resonant circuit current. Signals are demodulated from the reflected phase difference between the

Manuscript received March 11, 2022; revised May 2, 2022; accepted May 19, 2022. Date of publication May 30, 2022; date of current version June 24, 2022. This work was supported in part by the National Natural Science Foundation of China under Grants 51777210 and 62001301, in part by the Natural Science Foundation of Jiangsu Province under Grant BK20211246, and in part by the Project of Educational Commission of Guangdong Province of China under Grant 2021KTSCX276. Recommended for publication by Associate Editor R. Zane. *(Corresponding author: Chenyang Xia.)*

Chenyang Xia, Hongtai Zhang, Nan Wei, Shuze Zhao, Jiaan Yan, Xiangyu Song, and Zhijuan Liao are with the School of Electrical Engineering, China University of Mining and Technology, Xuzhou 221116, China (e-mail: 18260722082@163.com; 3465281940@qq.com; wn18852279016@163.com; 1171954566@qq.com; 1412371382@qq.com; ts19130201p31@cumt.edu.cn; zjliao@cumt.edu.cn).

Lijuan Xiang is with the School of Automotive and Transportation Engineering, Shenzhen Polytechnic, Shenzhen 518055, China (e-mail: lxiang@szpt.edu.cn).

Color versions of one or more figures in this article are available at https://doi.org/10.1109/TPEL.2022.3178998.

Digital Object Identifier 10.1109/TPEL.2022.3178998

inverter output voltage and the resonant current on the primary coil. Ishii *et al.* [13] used an automatic tuning assist circuit for frequency modulation, which enables simultaneous wireless power and signals transmission at multiple frequencies. The power carrier modulation technology is easy to realize, however, the signal transmission rate is limited by the power carrier, and the signal transmission will unavoidably lead to the output power fluctuation.

For the signal carrier wave injection simultaneous transmission technology, the high-frequency signal carrier is injected into the power transmission coil to achieve simultaneous power and signal transfer. In [14], the frequency division multiplexing technology is proposed to transmit power and signals through the shared coil. Fan *et al.* [15] realized the full-duplex communication and the signal transmission rate is up to 80 kb/s. Ji *et al.* [16] and Madzharov *et al.* [17] used signal carrier injection transformers to achieve simultaneous transmission of the power and signal. In [18] and [19], the passive bandpass and band-reject filters are designed to avoid severe crosstalk between the power and signal transmission. This method can easily achieve the reverse signal transmission, and the signal rate can be effectively improved, but the additional equipment for the high-frequency signal carrier generation is costly and the injecting signals will attenuate greatly through the wireless power transfer channel.

For the harmonic utilization simultaneous transmission technology, the harmonic in the system is used as the signal carrier to achieve the signal transmission. In [20] and [21], the triangular wave current is generated on the primary coil by removing the resonant capacitor on the primary side. The power and signal are transferred, respectively, through the fundamental and third components of the triangular current. In [22] and [23], the phase angle of the inverter is changed to produce a trapezoidal wave current on the primary coil. The harmonic utilization simultaneous transmission system is employed simply to realize signal transmission and stable power transmission without additional circuits. The power transfer efficiency is not affected because the power transfer channel is not changed.

As mentioned before, compared with the energy envelope modulated technology, the harmonic utilization technology can realize a higher signal transmission rate and reduce the output power fluctuation greatly. Compared with the signal carrier wave injection technology, the harmonic utilization technology reduces the volume and cost of the system. Therefore, harmonic utilization technology has attracted wide attention. However, the existing harmonic utilization technology can only transmit the serial signal, the low transmission rate fails to satisfy the communication requirements in the WPT system. Moreover, since the harmonic comes from the power transmission, the signal transmission strongly depends on the power transmission. When the demand for the power is changed on the load, the signal transmission will be affected and resulting in unsuccessful demodulation. The decoupling of the power and signals transmission will increase the flexibility of the WPT system.

To solve the problems in the current harmonic utilization technology, a simultaneous wireless power and multibit signals transfer (SWPMST) system with hybrid modulation waves

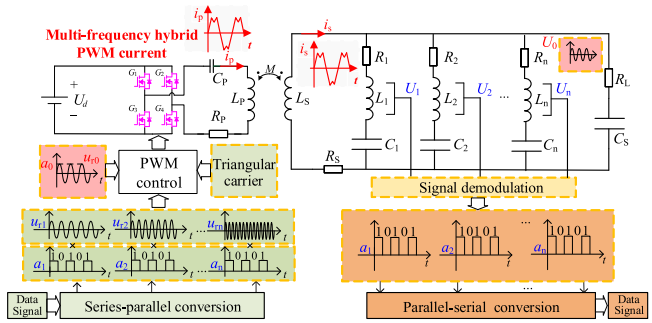

Fig. 1. SWPMST system with hybrid modulation waves PWM control.

pulsewidth modulation (PWM) control is proposed. Based on the multifrequency modulated PWM control technology [25], the simultaneous transmission of power and multibit signals are achieved successfully. The signal transmission rate is multiplied by two times through the realization of parallel signals transmission. The power and signals are modulated into the system through the modulation waves with different frequencies, so the signal transmission no longer depends on the power transfer. By optimizing system parameters, the interference between the power and signal transmission can be reduced, which increases the stability of the system.

II. Proposed SWPMST System

A. Structure and Parameters of SWPMST System With Hybrid Modulation Waves PWM Control

The structure of the SWPMST system with hybrid modulation waves PWM control is shown as Fig. 1.

In Fig. 1, L_{p}, L_{s} is the self-inductance of the transmitting and receiving coils separately. C_{p}, C_{s} is the resonant capacitor of the transmitting and receiving coils, respectively. R_{p}, R_{s} is the internal resistance of the transmitting and receiving coils, respectively. M is the mutual inductance between the two coils. R_{L} is the load, $L_{\mathrm{s}}, C_{\mathrm{s}}, R_{\mathrm{L}}$ forms the secondary side power transfer channel. $L_1, L_2, \ldots, L_{\mathrm{n}}$ are the detection inductance values of the n signal channels, $C_1, C_2, \ldots, C_{\mathrm{n}}$ are the resonant capacitor of the n signal channels. $R_1, R_2, \ldots, R_{\mathrm{n}}$ are the resistors of the n signal channels. L_1, C_1, R_1 forms the first signal transmission channel, L_2, C_2, R_2 forms the second signal transmission channel, …, L_{n}, $C_{\mathrm{n}}, R_{\mathrm{n}}$ forms the nth signal transmission channel.

The resonant frequency of the primary side circuit is f_0, the resonant frequencies of each signal channel are $f_1, f_2, \ldots, f_{\mathrm{n}}$. L_{p}, C_{p} constitute the frequency f_0 selection channel of the primary side, L_{s}, C_{s} constitute the frequency f_0 selection channel of the secondary side, L_1, C_1 constitute the frequency f_1 selection channel, L_2, C_2 constitute the frequency f_2 selection channel, L_{n}, C_{n} constitute the frequency f_{n} selection channel. The parameters of the multifrequency receiving network should be satisfied with

$$\begin{cases} (2\pi f_0)^2 L_P C_P = 1 \\ (2\pi f_0)^2 L_S C_S = 1 \\ (2\pi f_k)^2 L_k C_k = 1 \end{cases} \tag{1}$$

where ($1 \le k \le n$, $k \in Z^*$).

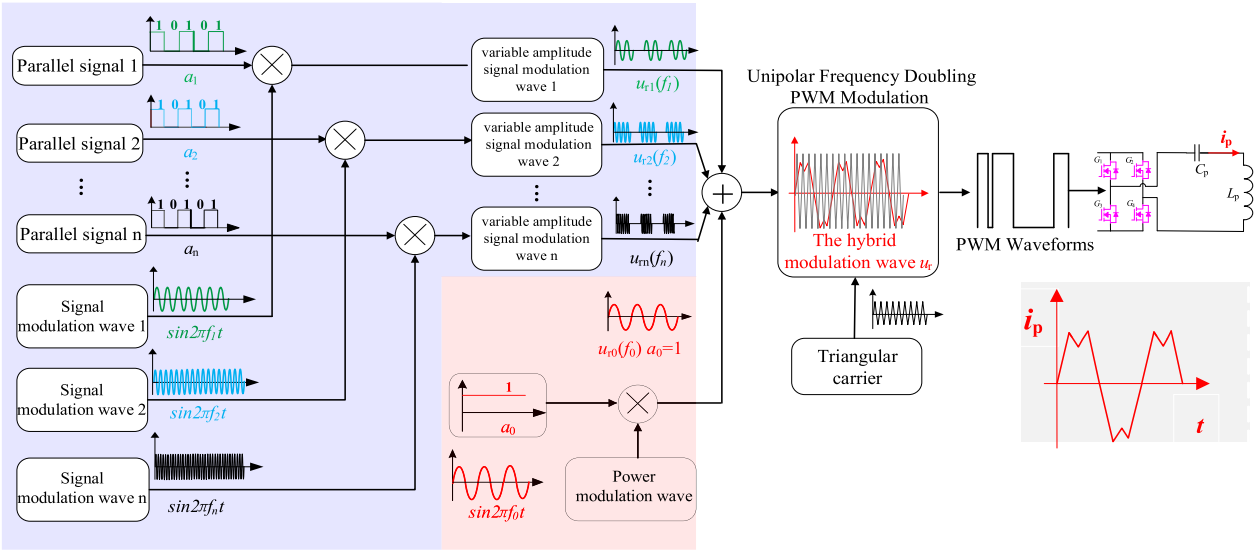

Fig. 2. Modulation of the power and signals.

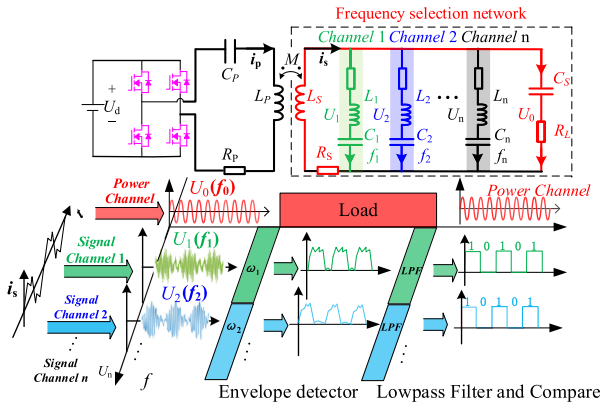

Fig. 3. Demodulation of the power and signals.

The carrier wave of the SWPMST with hybrid PWM control is a triangular wave in the inverter controller. The hybrid modulation wave u_r is a multiple sine waveform, which is superimposed by the sine waveforms of adjustable amplitude and frequency

$$u_r = u_{r0} + u_{r1} + \cdots + u_{rn} = a_0 \sin 2\pi f_0 t + a_1 \sin 2\pi f_1 t + \cdots + a_n \sin 2\pi f_n t. \quad (2)$$

u_{r0} is the modulation wave for power transfer, $u_{r1}, u_{r2}, \ldots, u_{rn}$ is the variable amplitude signals modulation waves for n signal transmission channels, and $a_0, a_1, a_2, \ldots, a_n$ is the amplitude of each modulation wave.

B. Working Principle of the SWPMST System With Hybrid Modulation Waves PWM Control

Based on the SWPMST system with hybrid modulation waves PWM control in Fig. 1, the modulation and demodulation of the power and signals are shown in Figs. 2 and 3.

The band signal is converted into n parallel transmission signals. In Fig. 2, based on the ASK modulation strategy, n parallel signals $(a_1, a_2, \ldots, a_n)$ are multiplied by the corresponding signal modulation waves with different frequencies $(f_1, f_2, \ldots, f_n)$. As a result, n parallel transmission signals are modulated into variable amplitude signal modulation waves $(u_{r1}, u_{r2} \ldots, u_{rn})$. Power transmission always exists, so the power modulation degree a_0 remains at 1. The power modulation degree a_0 is multiplied by the power modulation wave with frequency f_0, which produces the power modulation wave (u_{r0}). Then, the power modulation wave (u_{r0}) and n parallel variable amplitude signal modulation waves $(u_{r1}, u_{r2} \ldots u_{rn})$ are summed to produce the hybrid modulation wave u_r. The possible numbers of transfer bits n depend on the chosen carrier frequency and the selected modulation frequencies. According to the unipolar frequency doubling PWM modulation, the hybrid modulation wave is compared with the high-frequency triangular carrier wave (f_c), which produces the PWM waveform. The PWM waveforms are the driving pulse of the GaN inverter. Finally, the multifrequency hybrid PWM current i_p generates on the transmitting coil. The multifrequency hybrid PWM current includes the components of the power and n parallel transmission signals. By designing the proper parameters to avoid the crosstalk of the power and signals transmission, the power modulation degree a_0 can be adjusted to achieve a different power supply when the signals are transmitted stably. When the power transfer is unnecessary, the power modulation degree a_0 can be set to 0 and the signal modulation degree $(a_1, a_2, \ldots a_n)$ remains at the original value.

Based on the principle of mutual inductance coupling, the picking-up current i_s is induced shown in Fig. 3. The frequency selection network is formed by the power and signal transmission channels. Through the power transmission channel composed of L_s, C_s, and R_L, the power component with frequency f_0 is separated to supply the load R_L, thereby realizing the wireless power transfer. Through n signal transmission channels, the signal modulation wave components of the corresponding

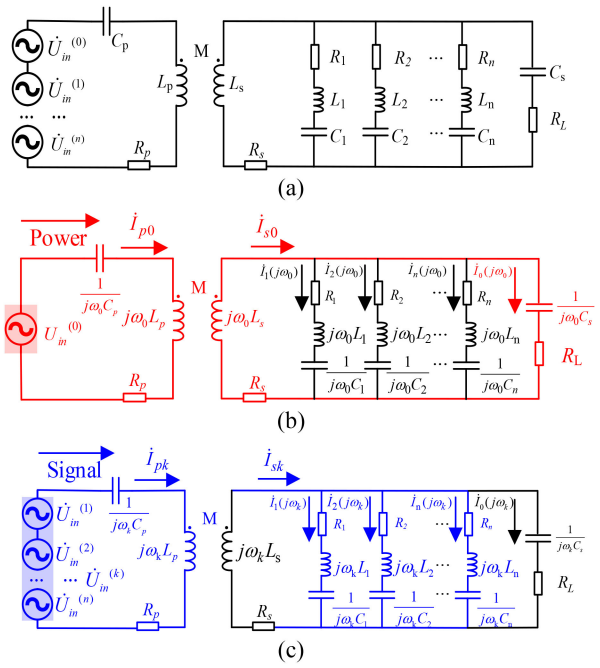

Fig. 4. System equivalent circuit. (a) SWPMST system. (b) Power transfer. (c) Signal transmission.

frequencies are obtained, respectively, thereby realizing the transmission of the *n*-bit signals of the system. The voltage on each detection inductance (U_1, U_2, …, U_n) are sampled into *n* signal demodulation circuits. The demodulation process is as follows: the voltage envelope on the detection inductance is obtained in the envelope detector, then high-frequency components of the voltage envelope are removed in the low pass filter (LPF). According to the comparison between the reference voltage and the voltage envelope, the multichannel signal demodulation is completed.

C. Power and Efficiency Derivation of the SWPMST System With Hybrid Modulation Waves PWM Control

According to the superposition theorem, the hybrid PWM current on the primary side can be approximated as the superposition of the power modulation wave frequency current and the signal modulation wave frequency current [25], which is shown in Fig. 4.

The equivalent circuit of the SWPMST system is shown in Fig. 4(a). According to the superposition theorem, it can be decomposed into the equivalent circuit under the frequency of the power modulation wave shown in Fig. 4(b) and the frequency of the signal modulation wave shown in Fig. 4(c). $\dot{U}_{in}^{(0)}$, $\dot{U}_{in}^{(k)}$, $\dot{I}_{p0}$, $\dot{I}_{pk}$, $\dot{I}_{s0}$, $\dot{I}_{sk}$, $\dot{I}_1(j\omega_0)$, $\dot{I}_1(j\omega_k)$, $\dot{I}_2(j\omega_0)$, $\dot{I}_2(j\omega_k)$,…, $\dot{I}_n(j\omega_0)$, $\dot{I}_n(j\omega_k)$, $\dot{U}_1(j\omega_0)$, $\dot{U}_1(j\omega_k)$, $\dot{U}_2(j\omega_0)$, $\dot{U}_2(j\omega_k)$,…, $\dot{U}_n(j\omega_0)$, $\dot{U}_n(j\omega_k)$, $\dot{I}_0(j\omega_0)$, $\dot{I}_0(j\omega_k)$, $\dot{U}_0(j\omega_0)$, $\dot{U}_0(j\omega_k)$ are the voltage on the primary side, the current on the transmitting coil, the current on the receiving coil, the current and voltage on the signal transmission channel numbered 1, 2, …, *n*, and load under the frequency of power modulation wave and the *k*th signal modulation wave, respectively.

In Fig. 4, the system under the power modulation wave frequency is analyzed when $m = 0$. The system under the *k*th signal modulation wave frequency is analyzed when $m = k$. The total impedance of the signal transmission network under the power and signal modulation wave $Z_n(j\omega_m)$, the impedance of the secondary side $Z_s(j\omega_m)$, and the input impedance of the system $Z_{in}(j\omega_m)$ are expressed as

$$\begin{cases} Z_n(j\omega_m) = \dfrac{1}{\sum\limits_{0\le m\le n,1\le k\le n}^{m,k}\left[1/\left(j\omega_m L_k + R_k + \frac{1}{j\omega_m C_k}\right)\right]} \\ Z_s(j\omega_m) = j\omega_m L_s + R_s + \dfrac{1}{1/Z_n(j\omega_m) + 1/\left(R_L + \frac{1}{j\omega_m C_s}\right)} \\ Z_{in}(j\omega_m) = \dfrac{(\omega_m M)^2}{Z_s(j\omega_m)} + R_p + j\omega_m L_p + \dfrac{1}{j\omega_m C_p}. \end{cases} \tag{3}$$

According to the unipolar frequency multiplication PWM modulation [25], the inverter output voltage is set as

$$\dot{U}_m = \frac{a_m U_d}{\sqrt{2}} \sin \omega_m t \tag{4}$$

where U_d represents the amplitude of the dc input voltage, and a_m represents the modulation degree under the corresponding modulation wave.

The current on the primary and secondary sides are, respectively, expressed as

$$\begin{cases} \dot{I}_p(j\omega_m) = \frac{\dot{U}_m}{Z_m} \\ \dot{I}_s(j\omega_m) = \frac{\dot{I}_p(j\omega_m)\cdot j\omega_m M}{Z_s(j\omega_m)}. \end{cases} \tag{5}$$

Due to the large component of the power modulation wave in the hybrid PWM current and the large equivalent impedance of the signal frequency selection channel, the signal detection channel can be ignored when calculating the power and efficiency under the power modulation wave. From (3)–(5), the power P_0 and efficiency η_0 of the proposed system under the power modulation wave frequency are calculated as follows:

$$P_0 = \left|\dot{I}_{s0}\right|^2 R_L \tag{6}$$

$$\eta_0 \approx \frac{\left|\dot{I}_{s0}\right|^2 R_L}{\left|\dot{I}_{p0}\right|^2 \mathrm{Re}\,(Z_0)} = \frac{(\omega_0 M)^2 R_L}{(R_L + R_s)^2 R_p + (R_L + R_s)(\omega_0 M)^2}. \tag{7}$$

III. Crosstalk Analysis of the SWPMST With Hybrid Modulation Waves PWM Control

To analyze the crosstalk characteristics of the SWPMST with hybrid modulation waves PWM control, the system parameters are shown in Table I, which are set in conjunction with the actual system.

A. Crosstalk From Signal Transmission to Power Reception

Considering the power modulation frequency selection channel in the actual system is not entirely ideal, trace amounts of signal modulation wave frequency components still exist on the load. The crosstalk voltage caused by signals transmission on the load should be taken into account.

TABLE I
SYSTEM PARAMETER CONFIGURATION TABLE

Parameters	Values	Parameters	Values
f_c	600.00 kHz	f_0	20.00 kHz
f_1	60.00 kHz	f_2	80.00 kHz
L_p	15.12 μH	L_s	37.30 μH
R_p	0.04 Ω	R_s	0.10 Ω
C_s	1.62 μF	C_p	4.03 μF
M	10.25 μH	R_1	1.00 Ω
R_2	0.50 Ω	a_0	0.70
a_1	0.30	a_2	0.30
L_1	427.13 μH	C_1	16.47 nF
L_2	385.76 μH	C_2	9.77 nF

According to Fig. 4, $\dot{U}_0(j\omega_0)$ and $\dot{U}_0(j\omega_k)$ are defined as the load voltage under the power and the kth signal modulation wave frequency, respectively. From (3)–(5), the load voltage under the power frequency and the kth signal channel corresponding frequency are obtained as

$$\begin{cases} \dot{U}_0(j\omega_0) = \frac{R_L}{R_L + \frac{1}{j k \omega_0 C_s}} \cdot \frac{Z_s'(j\omega_0)}{Z_s(j\omega_0)} \cdot \dot{I}_{p0}(j\omega_0) \cdot j\omega_0 M \\ \dot{U}_0(j\omega_k) = \frac{R_L}{R_L + \frac{1}{j\omega_k C_s}} \cdot \frac{Z_s'(j\omega_k)}{Z_s(j\omega_k)} \cdot \dot{I}_{pk}(j\omega_k) \cdot j\omega_k M \end{cases} \tag{8}$$

where $Z'_s(j\omega_m) = Z_s(j\omega_m) - (j\omega_m L_s + R_s)$, (m = 0 or k).

From (8), the crosstalk from the signal transmission to power reception is mainly related to the detection inductance value of the kth signal transmission channel L_k, the corresponding frequency of kth signal channel f_k, and the load resistance R_L.

Based on the parameters shown in Table I, when the frequency of the power transmission channel is 20 kHz and the frequency of two-bits signals transmission channel is, respectively, 60 kHz and 80 kHz, the crosstalk from the signal transmission to power reception is shown in Fig. 5. Among them, the load voltage curve under the power modulation wave frequency is shown in Fig. 5(a) and (b). The crosstalk voltage curve under the 60 kHz and 80 kHz signal modulation wave frequency is, respectively, shown in Fig. 5(c) and (d).

In Fig. 5(a) and (b), the load voltage under the power modulation wave frequency f_0 is related to the detection inductance L_k and load resistance R_L. When L_k is less than 10 μH, the load voltage under the power modulation wave frequency is greatly sensitive to the detection inductance L_k. When L_k is greater than 10 μH, the load voltage under the power modulation wave frequency tends to be stable. At the same time, with the load resistance increasing, the signal crosstalk voltage rises, and tends to be stable, which is up to 40 V. In Fig. 5(c) and (d), the signal crosstalk voltage is irrelevant to the detection inductance L_k. Moreover, the signal crosstalk voltage tends to be stable when R_L>20 Ω, the maximum value is 0.6 V and 0.09 V. The crosstalk of 60 kHz transmission channel for power transfer is a little larger than that of 80 kHz transmission channel, but they are much smaller than the load voltage under the power modulation wave frequency.

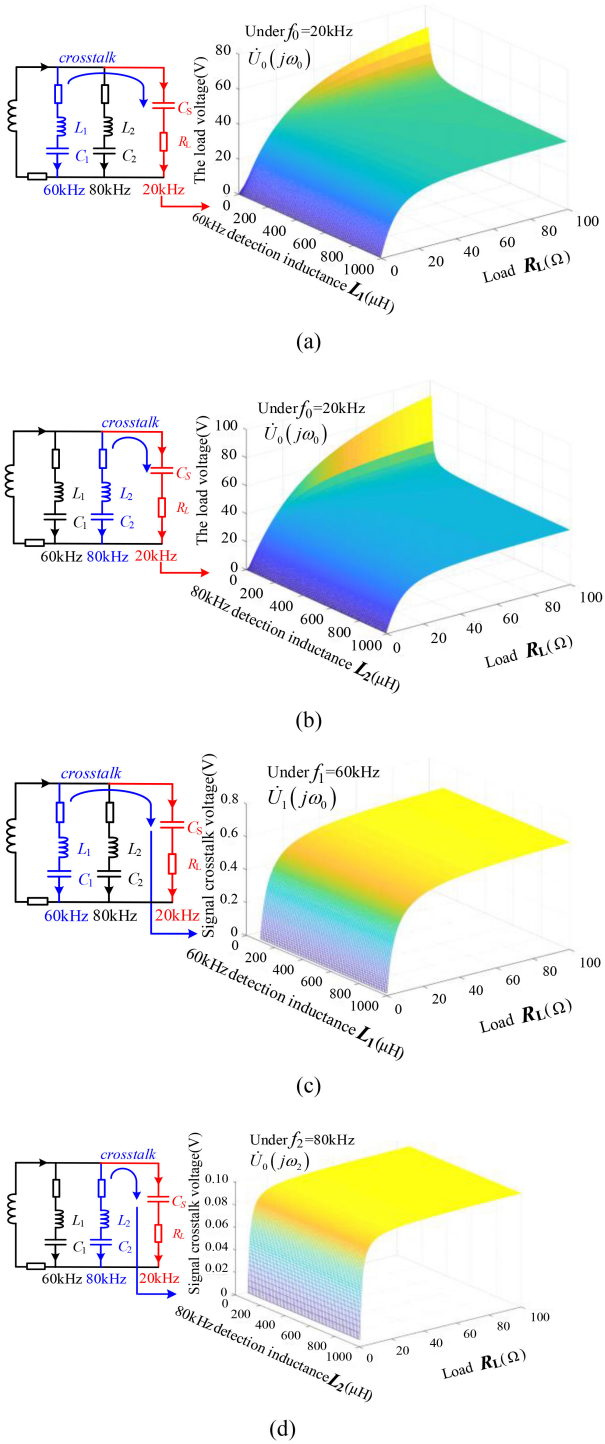

Fig. 5. Crosstalk from the signal transmission to power reception. (a) Voltage on the load varied with 60 kHz detection inductance L_1 under f_0 = 20 kHz. (b) Voltage on the load varied with 80 kHz detection inductance L_2 under f_0 = 20 kHz. (c) Signal crosstalk voltage on the load under f_1 = 60 kHz. (d) Signal crosstalk voltage on the load under f_2 = 80 kHz.

B. Crosstalk From Power Reception to Signal Transmission

The signal modulation frequency selection channel in the experiment is not ideal, some power modulation wave frequency components still exist in the signal transmission channels. The crosstalk voltage caused by the power reception should be analyzed to enable successful signal demodulation.

According to Fig. 4, $\dot{U}_k(j\omega_k)$ and $\dot{U}_k(j\omega_0)$ are, respectively, defined as the detection inductance voltage under the frequency of the kth signal modulation wave and power modulation wave.

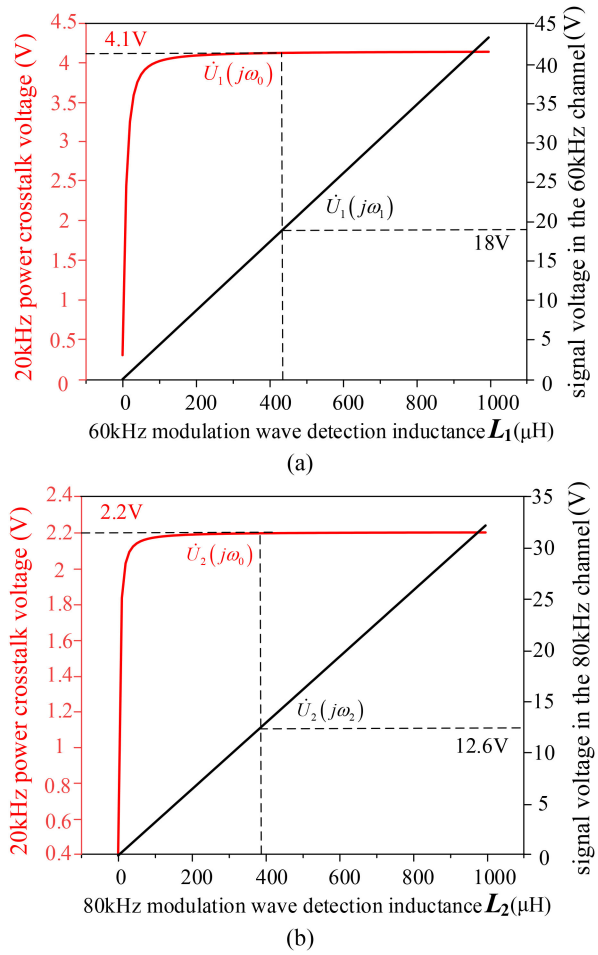

Fig. 6. Crosstalk from power reception to signal transmission. (a) Signal voltage in the 60 kHz channel and 20 kHz power crosstalk voltage. (b) Signal voltage in the 80 kHz channel and 20 kHz power crosstalk voltage.

From (3)–(5), the *k*th signal detection voltage under the power and *k*th signal modulation wave frequency is obtained as

$$\begin{cases} \dot{U}_k\left(j\omega_0\right)=\frac{j\omega_0 L_k}{R_k+j\omega_0 L_k+\frac{1}{j\omega_0 C_k}}\cdot\frac{Z_s'(j\omega_0)}{Z_s(j\omega_0)}\cdot\dot{I}_{\mathrm{p0}}\left(j\omega_0\right)\cdot j\omega_0 M \\ \dot{U}_k\left(j\omega_k\right)=\frac{j\omega_k L_k}{R_k+j\omega_k L_k+\frac{1}{j\omega_k C_k}}\cdot\frac{Z_s'(j\omega_k)}{Z_s(j\omega_k)}\cdot\dot{I}_{\mathrm{pk}}\left(j\omega_k\right)\cdot j\omega_k M. \end{cases} \tag{9}$$

The transfer function $G_1(\omega)$, $G_2(\omega)$ of the voltage on detection inductance L_1, L_2 is given by the

$$\begin{cases} G_1(\omega)=\frac{\dot{U}_1}{\dot{U}_{\mathrm{d}}} \\ G_2(\omega)=\frac{\dot{U}_2}{\dot{U}_{\mathrm{d}}} \end{cases} \tag{10}$$

where U_{d} is the dc supply voltage.

According to (9), the crosstalk from power reception to signal transmission is mainly related to the detection inductance value of the *k*th signal channel L_{k} and the corresponding frequency of *k*th signal channel f_{k}. When the frequency of the power transmission channel is 20 kHz and the frequency of the two-bits signals transmission channel is, respectively, 60 kHz and 80 kHz, based on the parameters shown in Table I, the crosstalk from power reception to signal transmission is shown in Fig. 6. Among them, the signal voltage in the 60 kHz channel and the power crosstalk voltage on the 60 kHz modulation wave detection inductance L_1 is shown in Fig. 6(a). Signal voltage in the 80 kHz channel and the power crosstalk voltage on the 80 kHz modulation wave detection inductance L_2 is shown in Fig. 6(b).

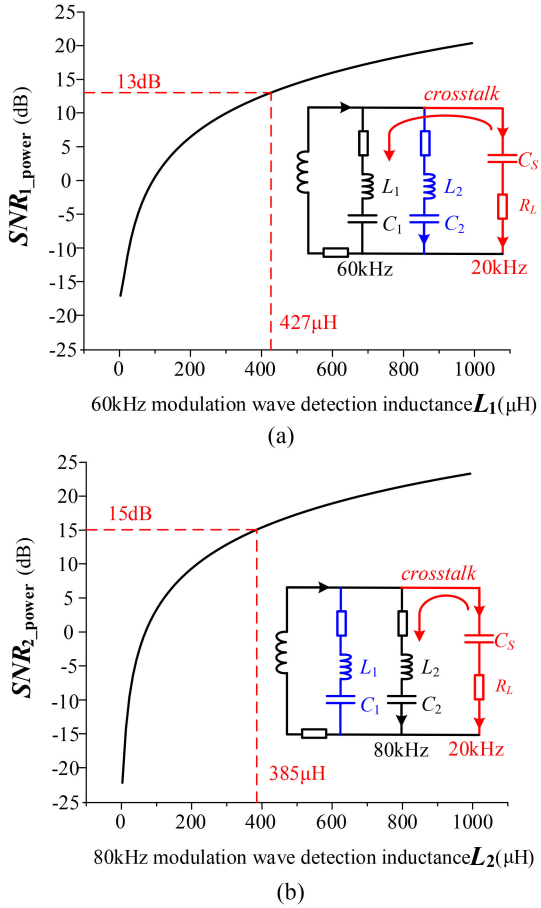

Fig. 7. $\mathrm{SNR}_{k\_\mathrm{power}}$ curve. (a) 60 kHz signal transmission channel $\mathrm{SNR}_{1\_\mathrm{power}}$. (b) 80 kHz signal transmission channel $\mathrm{SNR}_{2\_\mathrm{power}}$.

In Fig. 6, the crosstalk voltage caused by power reception tends to be stable with L_{k} increased. The signal voltage on the signal detection inductance is positively correlated with L_{k}.

Supposing that the impact of Gaussian white noise is ignored, the signal-to-noise ratio $\mathrm{SNR}_{k\_\mathrm{power}}$ of the signal transmission (the noise caused by power reception) in this system is defined as

$$\mathrm{SNR}_{k\_\mathrm{power}}=20\lg\left(\frac{\dot{U}_k\left(j\omega_k\right)}{\dot{U}_k\left(j\omega_0\right)}\right). \tag{11}$$

The $\mathrm{SNR}_{k\_\mathrm{power}}$ curves for the 60 kHz and 80 kHz transmission channels are plotted according to (11), as shown in Fig. 7.

In Fig. 7, the SNR of signal transmission (the noise caused by power reception) increases with the value of the detection inductance L_{k}. The crosstalk signal-to-noise ratio $\mathrm{SNR}_{1\_\mathrm{power}}$ and $\mathrm{SNR}_{2\_\mathrm{power}}$ of the two signals transmission channels can be adjusted to the proper value. When $L_1 = 427$ μH and $L_2 = 385$ μH shown as Table I, $\mathrm{SNR}_{1\_\mathrm{power}}$ and $\mathrm{SNR}_{2\_\mathrm{power}}$ are 13 dB and 15 dB, respectively.

C. Crosstalk Between Different Signal Transmission Channels

In reason of the transmission of the parallel signals, the crosstalk voltage caused by different signal transmission channels should be considered.

Making $a,b \in [1, n]$, $a \neq b$, ω_a is supposed to be the ath signal channel corresponding frequency, ω_b is supposed to be the bth signal channel corresponding frequency. $\dot{U}_a(j\omega_k)$ and $\dot{U}_b(j\omega_k)$ are, respectively, defined as detection inductance voltage in the ath and bth signal transmission channel under the ath signal channel corresponding frequency f_k. From (3)–(5), $\dot{U}_a(j\omega_k)$ and $\dot{U}_b(j\omega_k)$ can be expressed as

$$\begin{cases} \dot{U}_a(j\omega_a) = \frac{j\omega_a L_a}{R_a + jk\omega_a L_a + \frac{1}{j\omega_a C_a}} \cdot \frac{Z_s'(j\omega_a)}{Z_s(j\omega_a)} \cdot \dot{I}_{pk}(j\omega_a) \cdot j\omega_a M \\ \dot{U}_a(j\omega_b) = \frac{j\omega_b L_a}{R_a + j\omega_b L_a + \frac{1}{j\omega_b C_a}} \cdot \frac{Z_s'(j\omega_b)}{Z_s(j\omega_b)} \cdot \dot{I}_{pk}(j\omega_b) \cdot j\omega_b M. \end{cases} \tag{12}$$

The crosstalk between different signal transmission channels is mainly related to the detection inductance L_k and the corresponding frequency of kth signal channel f_k from (12).

On the conditions that the frequency of the transmission channel is 20 kHz and the frequency of two-bits signal transmission channels is, respectively, 60 kHz and 80 kHz, the crosstalk from different signal transmission channels is shown in Fig. 8. Among them, the signal voltage in the 60 kHz channel and crosstalk voltage from 80 kHz channel on the 60 kHz modulation wave detection inductance L_1 is shown in Fig. 8(a), the signal voltage in the 80 kHz channel and crosstalk voltage from 60 kHz channel on the 80 kHz modulation wave detection inductance L_2 is shown in Fig. 8(b).

Supposing that the impact of Gaussian white noise is ignored, the signal-to-noise ratio SNR_{k_signal} of different signal transmission channels (the noise caused by other signal transmissions) is defined as

$$\mathrm{SNR}_{k\_signal} = 20 \lg \left(\frac{\dot{U}_a(j\omega_k)}{\dot{U}_b(j\omega_k)} \right). \tag{13}$$

The SNR_{k_signal} curves (the noise caused by other signal transmissions) for the 60 kHz and 80 kHz transmission channels are plotted according to (13), as shown in Fig. 9.

In Fig. 9, the crosstalk signal-to-noise ratio SNR_{1_signal} and SNR_{2_signal} of the two signal transmission channels can be adjusted to the proper value. When $L_1 = 427$ μH and $L_2 = 385$ μH, the crosstalk voltage from the other signal transmission channel is separately 27 dB and 25 dB.

D. Discussion of the System Frequency Response

The attenuation characteristics of multisignals when transmitting via the coupling coils are mainly caused by the series resonance on the primary side, according to (3)

$$Z_p(j\omega_m) = R_p + j\omega_m L_p + \frac{1}{j\omega_m C_p}. \tag{14}$$

The frequency response of the series resonance on the primary side is shown in Fig. 10. In Fig. 10, the attenuation of the signals in the 60 kHz and 80 kHz channels transmitted via the coupling coils is, respectively, –14 dB and –17 dB.

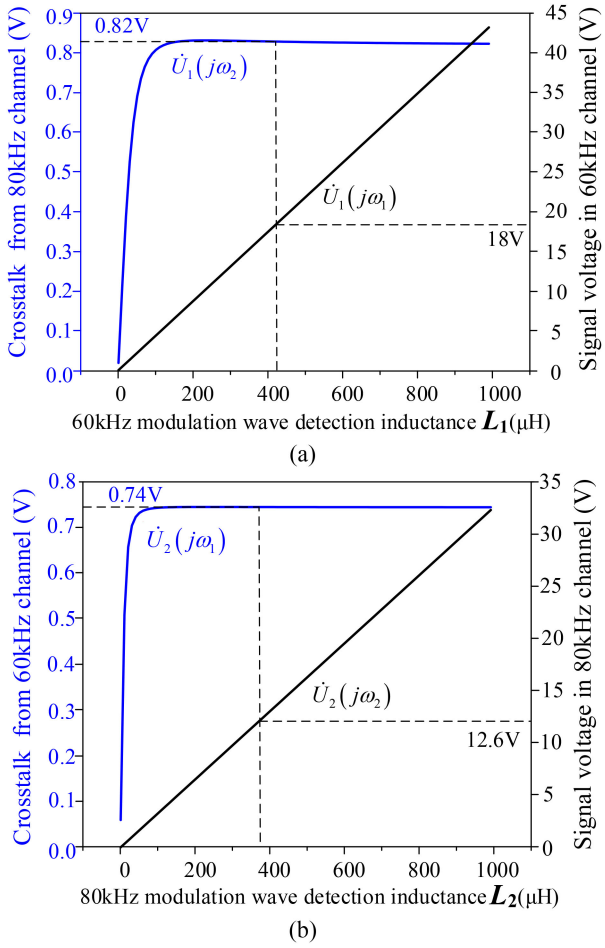

Fig. 8. Crosstalk between different signal transmission channels. (a) Signal voltage in the 60 kHz channel and crosstalk voltage from the 80 kHz channel. (b) Signal voltage in the 80 kHz channel and crosstalk voltage from the 60 kHz channel.

From (10), the frequency response of the signal detection inductances when transmitting signals of the 60 kHz and 80 kHz channels is displayed as Fig. 11.

It can be seen from Fig. 11 that when the frequency of the signal modulation wave is consistent with the resonant frequency of the signal receiving channel, the amplitude is the maximum. The gain of the 60 kHz and 80 kHz channels is 63 dB and 67 dB, which is much higher than the attenuation when transmitting via the coupling coils.

E. Selection of Power and Signal Transmission Frequencies

With the increase of the carrier ratio, the output voltage of the inverter is more accurate, but the great carrier ratio also means a high inverter switching frequency. According to [25], the carrier ratio of the power modulation wave is guaranteed to be an integer to avoid additional harmonic interference. In [25], the carrier ratio of the power modulation is set as 30 when the inverter switching frequency is 600 kHz. Therefore, we adopt the identical inverter switching frequency, and the frequency of the power modulation in this article is 20 kHz.

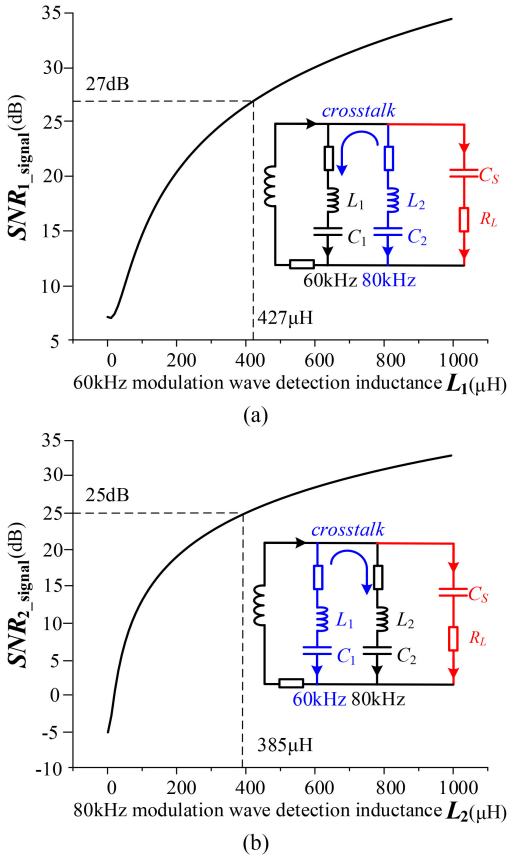

Fig. 9. $\mathrm{SNR}_{k\_\mathrm{signal}}$ curve of different L_k. (a) 60 kHz signal transmission channel $\mathrm{SNR}_{1\_\mathrm{signal}}$. (b) 80 kHz signal transmission channel $\mathrm{SNR}_{2\_\mathrm{signal}}$.

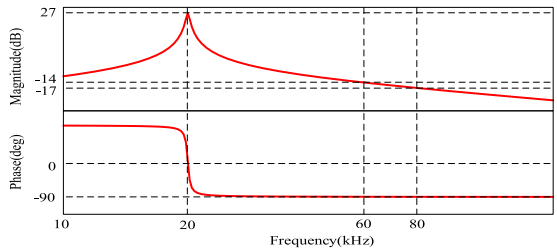

Fig. 10. Frequency response of the series resonance on the primary side.

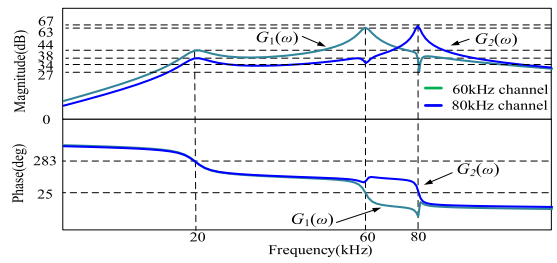

Fig. 11. Frequency response of the voltage on the signal channels.

When the detection inductance on the signal detection channel is always 427 μH, and the frequency of the power modulation wave is 20 kHz, the signal-to-noise ratio of the power reception for the different frequencies of the signal transmission channel is plotted according to (8) in Fig. 12.

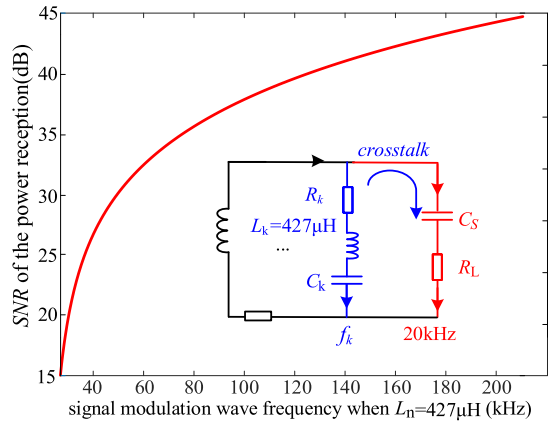

Fig. 12. Signal-to-noise ratio of the power reception for the different frequencies of the signal transmission channels.

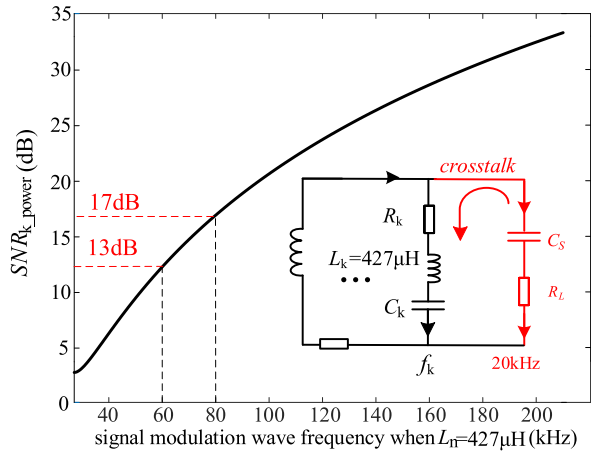

Fig. 13. Signal-to-noise ratio $\mathrm{SNR}_{k\_\mathrm{power}}$ of the signal transmission (the noise caused by power reception) for the different frequencies of the signal transmission channels.

In Fig. 12, with the frequency of the signal transmission channel increased, the signal-to-noise ratio of the power reception on the load is raised. The noise on the load is maintained at a relatively low level.

When the detection inductance on the signal detection channel is always 427 μH, the signal-to-noise ratio $\mathrm{SNR}_{k\_\mathrm{power}}$ of the signal transmission (the noise caused by power reception) for the different frequencies of the signal transmission channels is plotted according to (11) in Fig. 13. The signal-to-noise ratio $\mathrm{SNR}_{k\_\mathrm{signal}}$ of the 60 kHz signal transmission (the noise caused by other signal transmissions) for the different frequencies of the signal transmission channels is plotted according to (12) in Fig. 14.

In Fig. 13, on the premise that the signal detection channel is 427 μH, with the frequency of the signal transmission channels increased, the signal-to-noise ratio $\mathrm{SNR}_{k\_\mathrm{power}}$ of the signal transmission (the noise caused by power reception) is raised. The high frequency of the signal transmission channel is beneficial to reducing the crosstalk from the power reception.

In Fig. 14, the signal-to-noise ratio $\mathrm{SNR}_{k\_\mathrm{signal}}$ of the signal transmission (the noise caused by other signal transmissions)

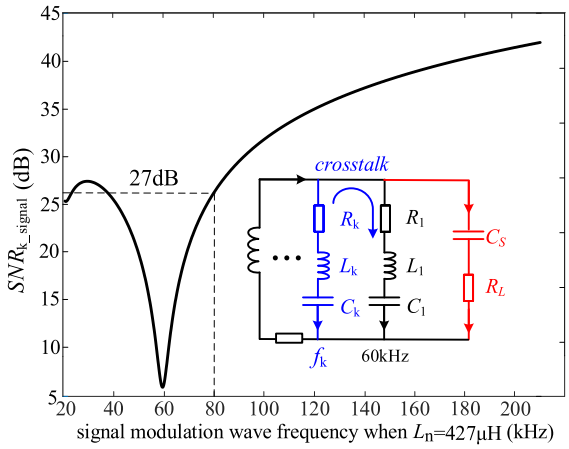

Fig. 14. Signal-to-noise ratio $\mathrm{SNR}_{k\_\mathrm{signal}}$ of the 60 kHz signal transmission (the noise caused by other signal transmissions) for the different frequencies of the signal transmission channels.

is sharply decreased when other signal channel frequency approaches 60 kHz.

In Figs. 13 and 14, adopting the high frequency of the signals transmission channel seems to be a useful method to reduce the crosstalk from power reception and other signal transmissions. However, the high frequencies of the signal modulation wave will cause great pressure on the inverter. The signal modulation frequencies should be appropriately lower than the switching frequency f_r.

From [23] and [26], to realize signals demodulation and constant output voltage on the load, the frequencies of power and signals transmission channel should satisfy the following requirements: 1) the high-level voltage envelope on the information detection inductor is twice of the low-level voltage envelope; 2) the load voltage fluctuation is less than 3%

$$\begin{cases} \dfrac{\left|\sum\limits_{i=1}^{n}\dot{U}_0(j\omega_k)\right|}{\left|\dot{U}_0(j\omega_0)\right|} \le 0.03 \\ \dfrac{\left|\dot{U}_k(j\omega_k)\right|}{\left|\dot{U}_k(j\omega_0)\right|+\left|\sum\limits_{i=1,i\neq k}^{n}\dot{U}_k(j\omega_i)\right|} \ge 2. \end{cases} \tag{15}$$

From (15), the crosstalk voltage on the load and the crosstalk voltage on the signal detection inductances should be restricted under the required value. The selection of the signal detection inductance and the frequencies of power and signal transmission channels should meet the crosstalk requirement.

IV. Signal Transmission Rate of the SWPMST With Hybrid Modulation Waves PWM Control

A. Relationship Between Signal Transmission Rate and Channel Numbers

The SWPMST with hybrid modulation waves PWM control is based on the principle of frequency division multiplexing. The schematic figure of SWPMST with hybrid modulation waves PWM control is shown as Fig. 15.

In Fig. 15, f_NRZ is the main bandwidth of the band signal assigned to each channel after serial-parallel conversion

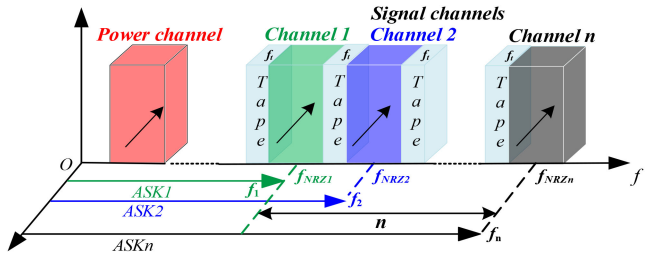

Fig. 15. Spectrogram of the SWPSMT with hybrid modulation waves PWM control.

($f_{\mathrm{NRZ1}} = f_{\mathrm{NRZ2}} = \cdots = f_{\mathrm{NRZn}}$), f_t is the signal spectrum isolation bandwidth to avoid interference between the different signal transmission channels. The ASK is used for the transmission of each parallel signal channel. Meanwhile, parallel signals separately are modulated by different modulation frequency waves (u_{r1}, $u_{\mathrm{r2}} \ldots u_{\mathrm{rn}}$) to avoid the crosstalk of the power and signal. With the development of GaN technology, the inverter switching frequency will improve greatly, which can increase the signal transmission channel numbers. The series signal transmission rate is n times as fast as the parallel signal transmission rate. The signal transmission rate theoretically can be multiplied by expanding the number of signal transmission channels. Moreover, the high frequency of the signal channel can reduce the signal transmission crosstalk from the power reception and other signal transmissions.

B. Relationship Between Signal Transmission Rate and Channel Parameter

According to Fig. 1, when the transition moment of the signal reach "0" and "1," the voltage change on L_k can be approximated as a zero-state response. The signal transmission rate will be limited by the response time [20]. From (1), the voltages on L_k and C_k are equivalent and opposite in direction. The transient equation on the signal channel is shown as

$$L_\mathrm{k}C_\mathrm{k}\frac{d^2u_\mathrm{Ck}}{dt^2} + R_\mathrm{k}C_\mathrm{k}\frac{du_\mathrm{Ck}}{dt} + u_\mathrm{Ck} = u_\mathrm{sk}(t) \tag{16}$$

where u_Ck is the voltage on the capacitor C_k, $u_\mathrm{sk}(t)$ is the voltage on the secondary coil, and $u_\mathrm{sk}(t) = \sqrt{2}U_\mathrm{k}\sin\omega_\mathrm{k}t$, its discriminant can be defined as

$$\Delta = {R_\mathrm{k}}^2 - \frac{4L_\mathrm{k}}{C_\mathrm{k}} < 0. \tag{17}$$

The system works on an under-damping state, and the capacitor voltage u_Ck transient process can be expressed as

$$u_\mathrm{Ck}(t) = u_\mathrm{sk}(t)\left[1 - \frac{1}{\omega_k\sqrt{L_kC_\mathrm{k}}}e^{-\frac{R_\mathrm{k}}{2L_k}t}\sin(\omega_k t + \varphi)\right]. \tag{18}$$

The transient process of signal reception is shown in Fig. 16, where $1/T_\mathrm{s}$ is the signal transmission rate and t_d is the duration of the transient process.

It is generally believed that the transient process gets to the end when the voltage amplitude in the transient process rises to

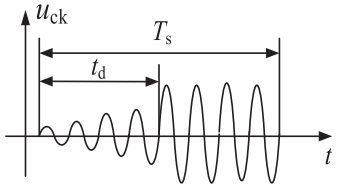

Fig. 16. Signal detection capacitor voltage transient process.

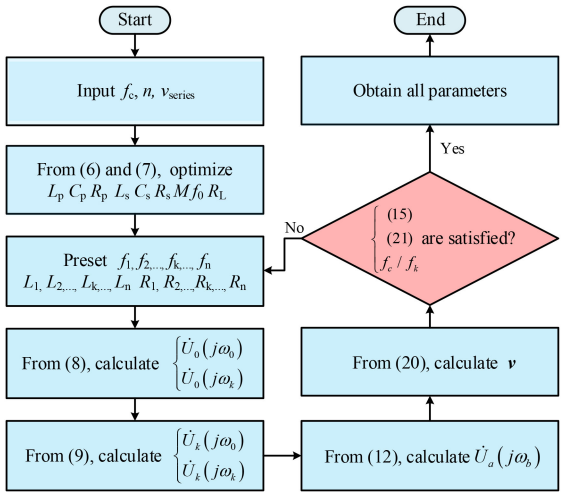

Fig. 17. Flow chart of the SWPMST system parameters design.

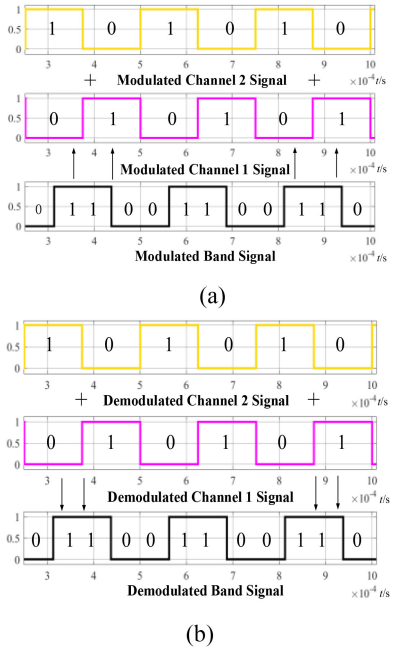

Fig. 18. Process of series-parallel/parallel-serial conversion. (a) Series-parallel conversion. (b) Parallel-serial conversion.

95%

$$e^{-\frac{R_k}{2L_k}t_d} = 0.05 \Rightarrow t_d = \frac{6L_k}{R_k}. \tag{19}$$

Neglecting the effects of other factors, the maximum communication rate v is defined as when $T_s = 2t_d$

$$v = \frac{n}{T_s} = \frac{nR_k}{12L_k}. \tag{20}$$

From (20), the signal transmission rate can be improved appropriately by increasing the resistance of the signal channel R_k or reducing the signal detection coil L_k. The maximum communication rate v should be larger than the series signal transmission rate v_{series}

$$v_{series} < v. \tag{21}$$

According to the crosstalk analysis and signal transmission rate analysis, the design flow chart of SWPMST system with hybrid modulation waves PWM control can be derived, as shown in Fig. 17.

The first step is to input the series signal transmission rate v_{series}, the signal channel numbers n, and the switching frequency f_c. The next step is to optimize the power and efficiency of the system by adjusting the appropriate electric parameters without the signal channels from formulas (6) and (7). The third step is to preset the frequencies of signal transmission channels and the value of the elements in the corresponding channels. Then calculate the power voltage and the crosstalk voltage from the signal transmission from (8). Besides, the signal voltage and the crosstalk voltage from power reception and other signal transmissions from (9) and (12) are obtained. Moreover, the maximum signal transmission rate v is given by (20). Finally, the calculation results of the previous steps should be examined by the crosstalk limitation (15), the signal transmission rate limitation (21), and the switching frequency f_c requirement. The carrier frequency f_c and the selected modulation frequencies f_k should be chosen under the consideration of the harmonics in the system and switching losses. If the requirement is satisfied, the system parameters are obtained, otherwise, the frequencies of signal transmission channels and the value of the elements in the corresponding channels need to be designed in step. 2 again.

V. Simulation and Experiment Verification

A. Simulation Module Verification

Based on the analysis abovementioned, a MATLAB/Simulink module is built to verify the correctness of the system. The band signal is formed by "011001100…," which is converted into "010101… …" as channel 1 and "101010…" as channel 2 (in a complementary form to channel 1). The simulation of the conversion process is shown in Fig. 18.

The modulation process of the power and signals is shown as Fig. 19.

In Fig. 19, the power modulation wave (u_{r0}) and the variable amplitude signal modulation waves (u_{r1}, u_{r2}) are sine waveforms with different frequencies (f_0, f_1, f_2). In period 1, the signal in the 60 kHz transmission channel is "1" and the 80 kHz transmission channel is "0," the hybrid modulation wave u_r includes the components of the 20 kHz power modulation wave and the 60 kHz modulation wave. In period 2, the signal in the 60 kHz transmission channel is "0" and the 80 kHz transmission channel is "1," the hybrid modulation wave u_r includes the components of the 20 kHz power modulation wave and the 80 kHz modulation

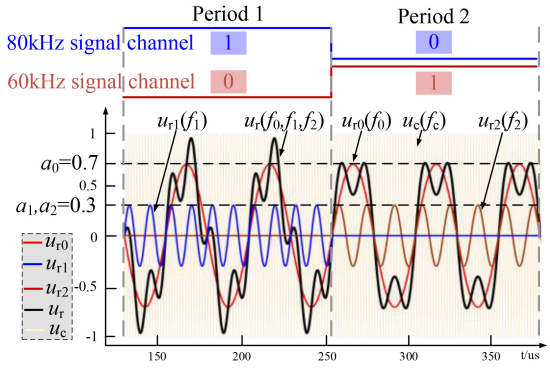

Fig. 19. Process of the power and signal modulation.

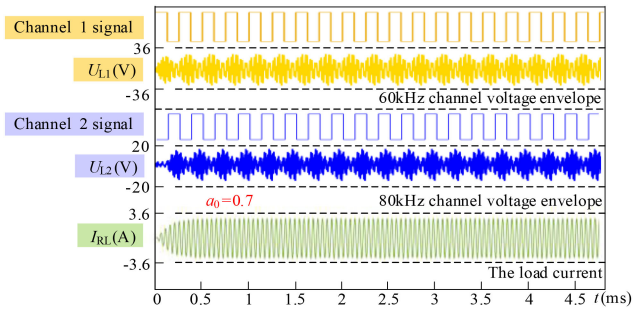

Fig. 20. Simultaneous power and two-bit signals transfer (60 kHz and 80 kHz channel).

TABLE II
ADJUSTED SYSTEM PARAMETER TABLE

Parameters	Values	Parameters	Values
f_1'	100.00 kHz	f_2'	120.00 kHz
f_c	600.00 kHz	n	2
R_1'	10.00 Ω	R_2'	15.00 Ω

wave. The components of the hybrid modulation wave depend on the transmitted signals.

From Table I, the load current and signals voltage envelope (60 kHz and 80 kHz channel) are shown in Fig. 20.

In Fig. 20, the signal voltage envelope can form stably when the power is transferred. Therefore, the system can achieve simultaneous power and signal transfer, however, the crosstalk noise from the power transfer to signal transmission is kind of serious. According to Fig. 13, the crosstalk can be decreased with the frequencies of the signal modulation waves raised. Therefore, the following parameters are adjusted, which are shown in Table II.

From Table II, the load current and signals voltage envelope (100 kHz and 120 kHz channel) are shown in Fig. 21.

Compared to Figs. 20 and 21, the crosstalk from the power to signal transmission is greatly reduced, and the simulation can prove the correctness of the crosstalk analysis.

The decoupling control of the power and signals is shown in Fig. 22.

In Fig. 22, the voltage envelope can keep steady when controlling the output voltage on the load by adjusting the power modulation degree a_0 from 0.7–0.6.

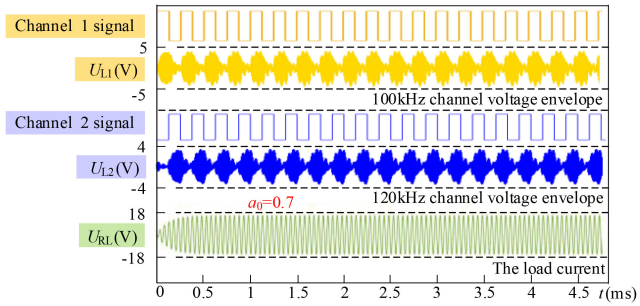

Fig. 21. Simultaneous power and two-bit signals transfer (100 kHz and 120 kHz channel).

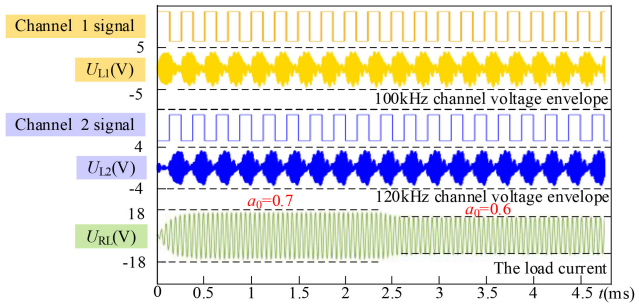

Fig. 22. Decoupling control of power and signals (100 kHz and 120 kHz channel).

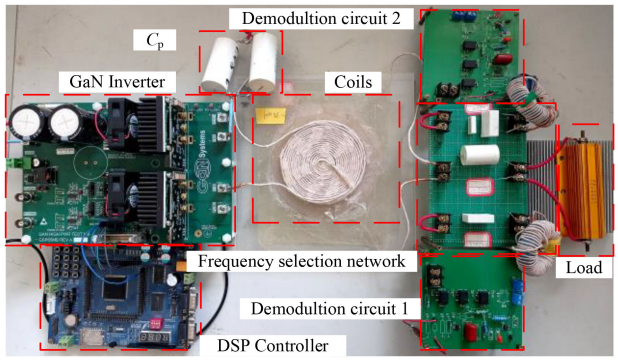

Fig. 23. Experimental platform.

B. Experimental Verification

To verify the correctness and effectiveness of the SWPMST with hybrid modulation waves PWM control, according to the parameters in Tables I and II, an experimental platform of the SWPMST with hybrid modulation waves PWM control was built shown in Fig. 23. The modulation process shown in Fig. 2 is realized in the DSP controller without any extra circuit.

The signal modulation frequency selection channel filters according to the frequency of the signal modulation wave. When the signal amplitude is "1," a relatively high amplitude voltage is generated on the detection inductance L_k. The demodulation circuit is shown in Fig. 24.

The design principle is as follows: the voltage on the detection inductance L_k is divided and converted as the input of the voltage follower formed by OPA2354. The envelope detector is formed by the detection diode D_1, the capacitor C_{d1}, and the resistance

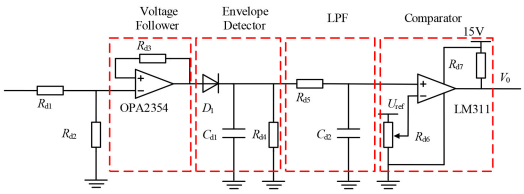

Fig. 24. Demodulation circuit.

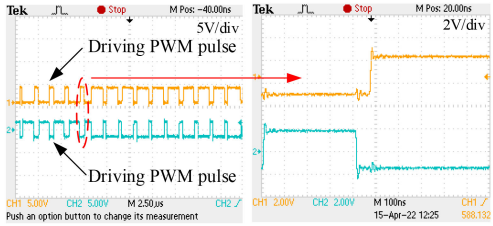

Fig. 25. Driving pulse of the GaN inverter.

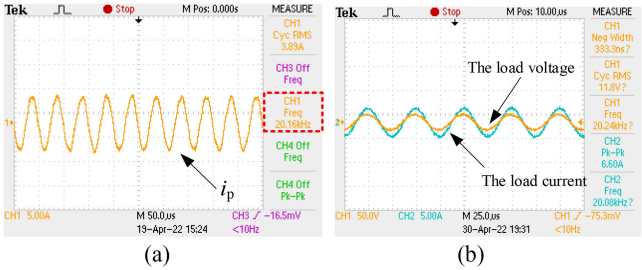

Fig. 26. Power transfer (a) i_{p}. (b) load voltage and current.

R_{d4}. After detecting the envelope, the signal is received in LPF. The signal demodulation is finally realized by the comparator consisting of LM311.

C. Power Characteristic Analysis

To analyze the power characteristics of the SWPMST with hybrid modulation waves PWM control, the driving pulse of the GaN inverter was measured, as shown in Fig. 25.

In Fig. 25, the driving pulse is generated by comparing the hybrid modulation wave u_{r} with the high-frequency triangular carrier wave. The waveform conforms to the unequal width characteristic of the typical PWM wave. Meanwhile, the ringing noise is relatively low and it has little effect on the signal transmission. The ringing noise of the switchers is mainly caused by the parasitic inductance and capacitance of the printed circuit board. From the user's guide of the GaN inverter, the ringing noise can be decreased by optimizing parameters in the drive circuit.

To analyze the power transmission characteristics of the SWPMST with hybrid modulation waves PWM control, the current in the primary coil i_{p}, and the waveform on the load are shown in Fig. 26.

In Fig. 26(a), i_{p} contains most of the power transfer components (20 kHz). In Fig. 26(b), the load voltage and current perform excellent quality with little total harmonic distortion.

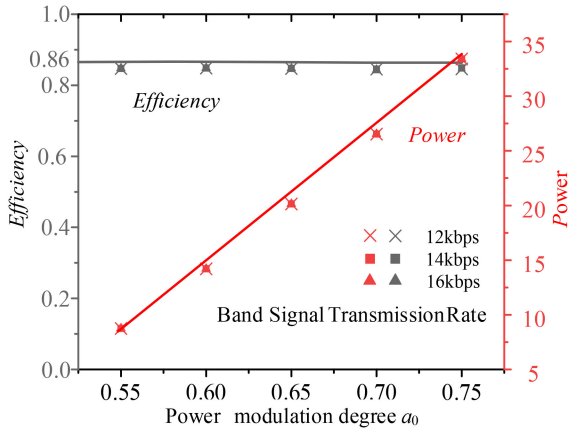

Fig. 27. Measured power and efficiency when the power modulation degree changed.

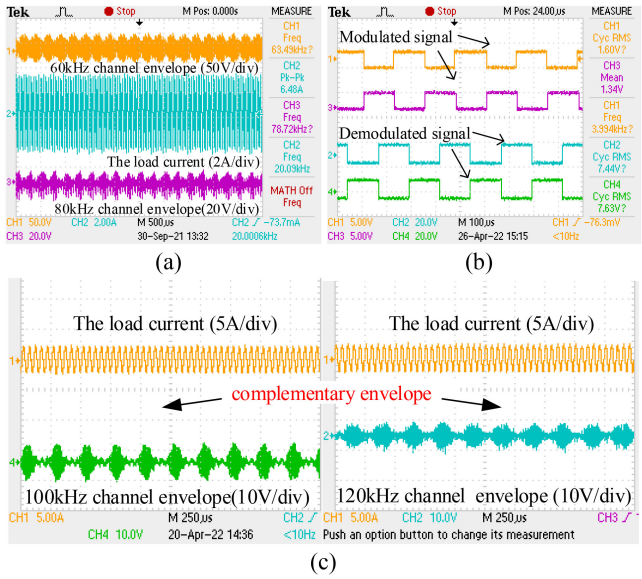

Fig. 28. Signal detection channel waveforms during power transfer. (a) 60 kHz and 80 kHz signal detection voltage envelope and load current. (b) Comparison of two-bits signal transmission. (c) 100 kHz and 120 kHz signal detection voltage envelope and load current.

To analyze the impact of signal transmission on the system power and efficiency, band signals with different rates of 12, 14, and 16 kb/s were sent. According to (6) and (7), the power and efficiency of the system were measured when the power modulation degree a_0 and band signal rates changed. The results are shown in Fig. 27.

The solid line in Fig. 27 is the theoretical curve of power and efficiency varied with power modulation degree a_0. The sets of discrete points are the actual power and efficiency when sending different data strings. In Fig. 27, the signal transmission has little impact on the system efficiency with different transmission rates. The theoretical efficiency of the system is 86.67% by (7), and the actual efficiency remains stable with the increase of the power modulation amplitude a_0, around 84%. The power on the load upgrade with the increase of the power modulation amplitude a_0. Therefore, the SWPMST with hybrid modulation waves PWM

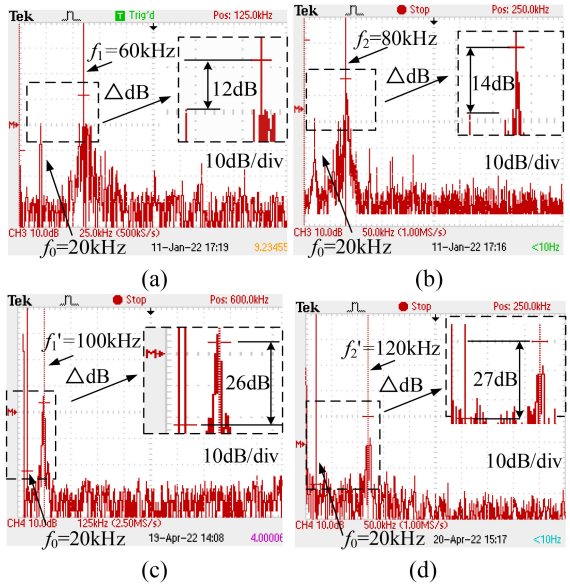

Fig. 29. Spectrums analysis. (a) 60 kHz channel. (b) 80 kHz channel. (c) 100 kHz channel. (d) 120 kHz channel.

control proposed in this article can realize the power transfer, and the transmission of the signals has little effect on the efficiency of the system.

D. Band Signal Transmission Analysis

Fig. 28 shows the experimental waveforms when transmitting the signal "011001100 …".

Fig. 28(a) shows the load current and voltage envelope on the detection inductance of the signal channel. The current on the load is stable when transmitting the signals. Fig. 28(b) presents a comparison of the 60 kHz and 80 kHz signal channel simultaneous transmission. In Fig. 28(a) and (b), the signals can be demodulated successfully, but there is rich noise on the voltage envelope. According to Table II, the adjusted signal channel frequencies are adopted. In Fig. 28(c), the crosstalk noise on the voltage envelope is decreased greatly.

The spectrums of the 60, 80, 100, and 120 kHz channels are analyzed in Fig. 29.

In Fig. 29(a) and (b), 60 kHz and 80 kHz constitute the main components of the whole spectrum and the main crosstalk noise comes from the power transfer (20 kHz). The signal-to-noise ratio from the 60 kHz signal transmission channel to the 20 kHz power reception channel is 12 dB, and the theoretical value is 13 dB from Fig. 7(a). The signal-to-noise ratio from the 80 kHz signal transmission channel to the 20 kHz power reception channel is 14 dB, and the theoretical value is 15 dB from Fig. 7(b). In Fig. 29(c) and (d), with the signal channel frequencies increased, the SNR of the signal transmission channels is improved greatly. The SNR of the signal transmission channels has been improved from 12/14–26/27 dB. Therefore, the correctness of the SWPMST with hybrid modulation waves PWM control proposed in this article is verified.

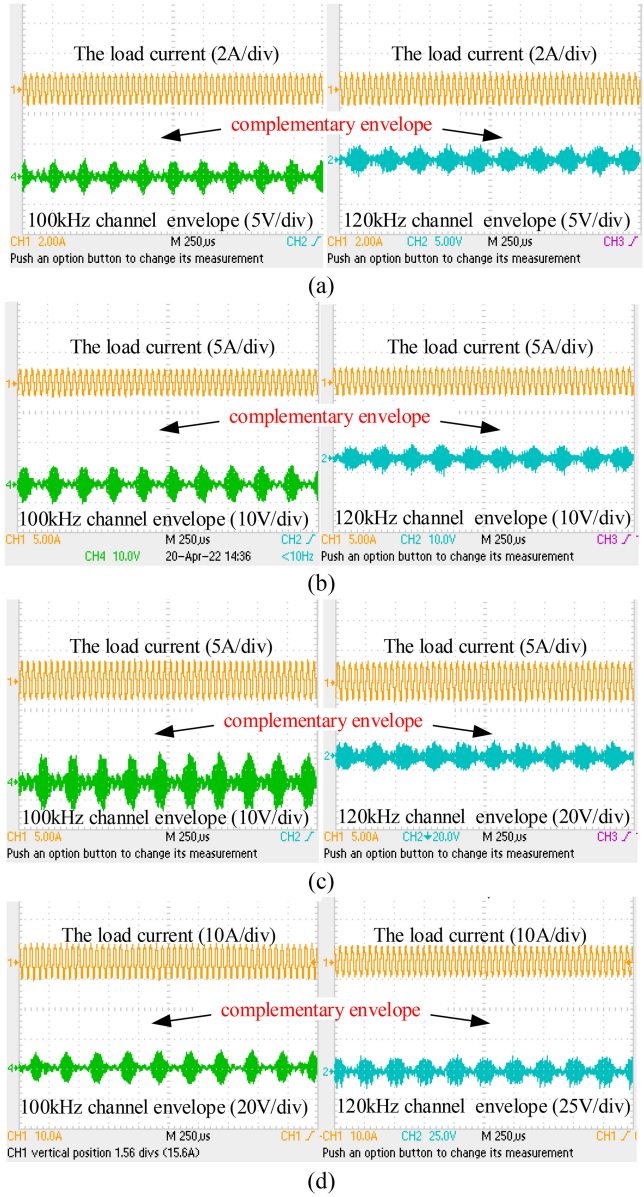

Fig. 30. 100 kHz and 120 kHz signal channel envelope with input voltage varied. (a) $U_{\mathrm{d}} = 5$ V. (b) $U_{\mathrm{d}} = 10$V. (c) $U_{\mathrm{d}} = 15$ V. (d) $U_{\mathrm{d}} = 20$ V.

When the input voltage and load are varied, the voltage envelope of 100 kHz and 120 kHz channels is shown in Figs. 30 and 31.

In Figs. 30 and 31, the voltage envelope can maintain stably when the input voltage and load are adjusted.

The decoupling control of the power and signals is shown in Fig. 32.

The decoupling control of the power and signal transmission is shown in Fig. 32. In Fig. 32(a) and (b), the power and signal can transfer independently. In Fig. 32(c), in the process of the power control, the 100 kHz and 120 kHz signal detection inductance voltage envelope keeps stable and the signal can be demodulated successfully. Therefore, the decoupling control of the power and signal transmission can be achieved in the proposed system.

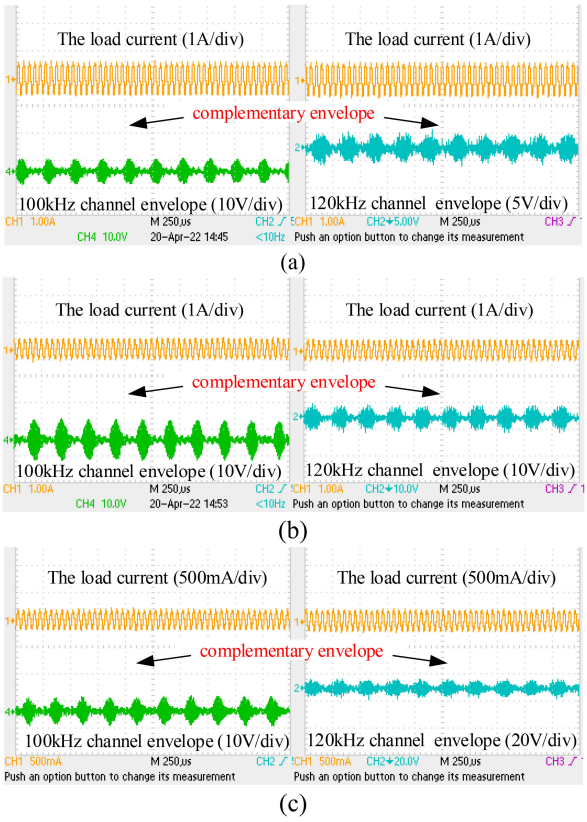

Fig. 31. 100 kHz and 120 kHz signal channel envelope with the load varied. (a) $R_L = 10\ \Omega$. (b) $R_L = 25\ \Omega$. (c) $R_L = 50\ \Omega$.

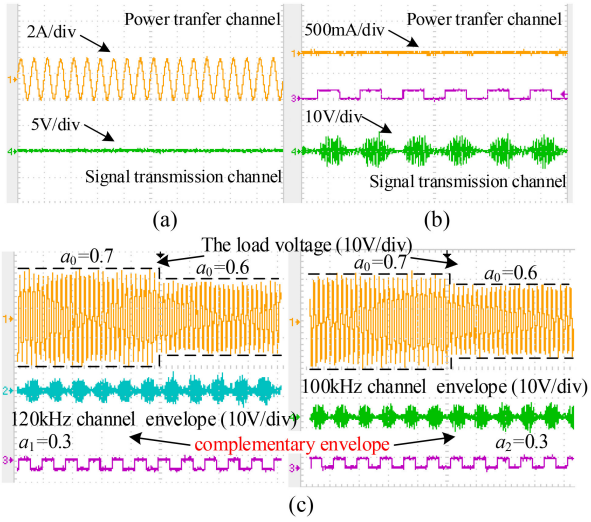

Fig. 32. Decoupling control of the power and two-bit signals transmission (100 kHz and 120 kHz signal channel). (a) Power transfer without signal transmission. (b) Signal transmission without power transfer. (c) $a_0 = 0.7$ convert to $a_0 = 0.6$.

E. Power Factor Analysis

To analyze the power factor in the system, the relationship between the power factor and the power modulation amplitude was measured, as shown in Fig. 33.

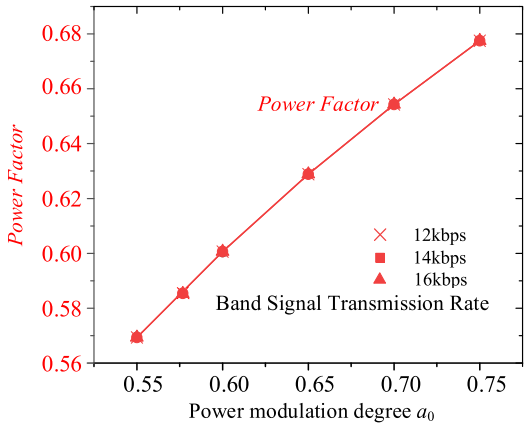

Fig. 33. Power factor with the power modulation degree changed.

TABLE III
EXISTING TECHNIQUES PRESENTED IN THE LITERATURE

Reference	[10]	[17]	[23]	This article
Transmission mode	Energy modulating	Carrier injection	Harmonic utilization	PWM modulating
Carrier frequency	N/A	1.47 MHz	N/A	60/80/100/120 kHz
Power factor	N/A	N/A	0.2	0.68
crosstalk	low	Relatively low	Relatively low	Relatively low
Bit rate	10 kb/s	19.2 kb/s	6 kb/s	16 kb/s
Channel numbers	1	1	1	2
Complexity	simple	complex	Relatively simple	simple
Decoupling control	No	N/A	No	Yes

In Fig. 33, the power factor is positively related to the power modulation degree, and the proposed system can be adaptable for different signal transmission rates.

To analyze the innovation of the proposed method in this article, the results are compared with existing technology presented in the literature, as shown in Table III.

From Table III, the SWPMST with hybrid modulation waves PWM control can realize high transmission power efficiency, relatively low crosstalk, and simple design cost. Compared to the paper [23], the power factor and signal transmission rate of this article have been improved obviously.

VI. CONCLUSION

The SWPMST with hybrid modulation waves PWM control is proposed in this article. PWM control of multifrequency hybrid modulation waves is used to transfer power and multibit signals, the power transfer channel, and the signal detection channels are separately formed on the secondary side. Based on the multi-frequency modulated PWM control technology, stable voltage envelopes can be detected on the signal detection inductance with little impact on power transmission. Finally, the envelope detection circuit is designed to complete the demodulation of the signals. The experimental results can prove the correction of

the simultaneous power and multibit signals transfer technology. Meanwhile, the signal transmission rate is also increased. The method proposed in this article retains the advantages in [23] while overcoming some shortcomings.

1) Increase signal transmission rate by realizing the parallel signal transmission.
2) Realize the decoupling control of transfer signals and power.
3) Greatly improve the power factor of the system.

However, this article still has the following shortcomings, which need to be further improved and perfected: the SWPMST with hybrid modulation waves PWM control in this article transmits signals from the primary side to the secondary side, the transmission of the multibit signals in the reverse direction needs to be further studied and realized. Moreover, the high switching frequency will cause switching losses.

REFERENCES

[1] H. Kim, H. Hirayama, S. Kim, K. J. Han, R. Zhang, and J. Choi, "Review of near-field wireless power and communication for biomedical applications," *IEEE Access*, vol. 5, pp. 21264–21285, 2017.

[2] S. Rao and J. Chiao, "Body electric: Wireless power transfer for implant applications," *IEEE Microw. Mag.*, vol. 16, no. 2, pp. 54–64, Mar. 2015.

[3] J. H. Kim *et al.*, "Development of 1-MW inductive power transfer system for a high-speed train," *IEEE Trans. Ind. Electron.*, vol. 62, no. 10, pp. 6242–6250, Oct. 2015.

[4] D. H. Tran, V. B. Vu, and W. Choi, "Design of a high-efficiency wireless power transfer system with intermediate coils for the on-board chargers of electric vehicles," *IEEE Trans. Power Electron.*, vol. 33, no. 1, pp. 175–187, Jan. 2018.

[5] J. Besnoff, M. Abbasi, and D. S. Ricketts, "High data-rate communication in near-field RFID and wireless power using higher order modulation," *IEEE Trans. Microw Theory*, vol. 64, no. 2, pp. 401–413, Jan. 2016.

[6] H. Lee, Y. Kim, J. H. Ahn, M. Y. Chung, and T. -J. Lee, "Wi-Fi and wireless power transfer live together," *IEEE Commun. Lett.*, vol. 22, no. 3, pp. 518–521, Mar. 2018.

[7] W.-S. Lee, S. Park, J.-H. Lee, and M. M. Tentzeris, "Longitudinally 'misalignment-insensitive dual-band wireless power and data transfer systems for a position detection of fast-moving vehicles," *IEEE Trans. Antennas Propag.*, vol. 67, no. 8, pp. 5614–5622, Aug. 2019.

[8] E. G. Kilinc *et al.*, "A system for wireless power transfer and data communication of long-term bio-monitoring," *IEEE Sens. J.*, vol. 15, no. 11,pp. 6559–6569, Nov. 2015.

[9] C. Yu, R. Lu, C. Su, and C. Zhu, "Study on wireless energy and data transmission for long-range projectile," *IEEE Trans. Plasma Sci.*, vol. 41, no. 5, pp. 1370–1375, May 2013.

[10] Y. Son and B. Jang, "Simultaneous data and power transmission in resonant wireless power system," in *Proc. Asia-Pacific Microw. Conf. Proc.*, 2013, pp. 1003–1005.

[11] G. Yilmaz, O. Atasoy, and C. Dehollain, "Wireless energy and data transfer for in-vivo epileptic focus localization," *IEEE Sensors J.*, vol. 13, no. 11, pp. 4172–4179, Nov. 2013.

[12] H. Li, S. Chen, J. Fang, and Y. Tang, "Synchronous rectification-based phase shift keying communication for wireless power transfer systems," in *Proc. IEEE 4th Southern Power Electron. Conf.*, 2018, pp. 1–4.

[13] M. Ishii, K. Yamanaka, and M. Sasaki, "Multiple FSK data and power transmission system using magnetic resonance wireless power transfer," in *Proc. IEEE Wireless Power Transfer Conf.*, 2019, pp. 208–211.

[14] J. Wu, C. Zhao, Z. Lin, J. Du, Y. Hu, and X. He, "Wireless power and data transfer via a common inductive link using frequency division multiplexing," *IEEE Trans. Ind. Electron.*, vol. 62, no. 12, pp. 7810–7820, Dec. 2015.

[15] Y. Fan, Y. Sun, X. Dai, Z. Zuo, and A. You, "Simultaneous wireless power transfer and full-duplex communication with a single coupling interface," *IEEE Trans. Power Electron.*, vol. 36, no. 6, pp. 6313–6322, Jun. 2021.

[16] L. Ji, L. Wang, C. Liao, and S. Li, "Simultaneous wireless power and bidirectional information transmission with a single-coil, dual-resonant structure," *IEEE Trans. Ind. Electron.*, vol. 66, no. 5, pp. 4013–4022, May 2019.

[17] N. Madzharov, R. Ilarionov, and L. Petkov, "Experimental studies of a method of simultaneous contactless transmission of energy and information signals through a common inductive link," in *Proc. IEEE XXVIII Int. Sci. Conf. Electron.*, 2019, pp. 1–4.

[18] Y. Sun, P. Yan, Z. Wang, and Y. Luan, "The parallel transmission of power and data with the shared channel for an inductive power transfer system," *IEEE Trans. Power Electron.*, vol. 31, no. 8, pp. 5495–5502, Aug. 2016.

[19] H. Kong, K. Feng, J. Wu, N. Jin, S. He, and J. Tao, "A novel conception of SWIPT system considering information independent transmission," in *Proc. IEEE/CIC Int. Conf. Commun. Workshops China*, 2019, pp. 200–203.

[20] C. Xia, R. Jia, Y. Wu, Q. Yu, and Y. Zhou, "WPIT technology based on the fundamental-harmonic component for a single-channel and two-coil ICPT system," *IET Power Electron.*, vol. 12, pp. 2608–2614, 2019.

[21] Z. Yan, Z. Xiang, L. Wu, and B. Wang, "Study of wireless power and information transmission technology based on the triangular current waveform," *IEEE Trans. Power Electron.*, vol. 33, no. 2, pp. 1368–1377, Feb. 2018.

[22] Y. Zhou, W. Lin, and B. Wang, "High-Efficiency coupling-insensitive wireless power and information transmission based on the phase-shifted control," *IEEE Trans. Power Electron.*, vol. 33, no. 9, pp. 7821–7831, Sep. 2018.

[23] C. Xia, R. Jia, Y. Shi, A. P. Hu, and Y. Zhou, "Simultaneous wireless power and information transfer based on phase-shift modulation in ICPT system," *IEEE Trans. Energy Convers.*, vol. 36, no. 2, pp. 629–639, Jun. 2021.

[24] P. Wang, Y. Sun, Y. Feng, T. Feng, Y. Fan, and X. Li, "An improvement of SNR for simultaneous wireless power and data transfer system with full-duplex communication mode," *IEEE Trans. Power Electron.*, vol. 37, no. 2, pp. 2413–2424, Feb. 2022.

[25] C. Xia, N. Wei, H. Zhang, S. Zhao, Z. Li, and Z. Liao, "Multifrequency and multiload MCR-WPT system using hybrid modulation waves SPWM control method," *IEEE Trans. Power Electron.*, vol. 36, no. 11, pp. 12400–12412, Nov. 2021.

[26] X. Liu, C. Xia, X. Han, Z. Wu, and Z. Liao, "Simultaneous wireless power and information transmission based on harmonic characteristic of soft-switching inverter," *IEEE Trans. Ind. Electron.*, vol. 69, no. 6, pp. 6090–6100, Jun. 2022.

Chenyang Xia (Member, IEEE) was born in Jiangsu Province, China, in 1982. He received the B.S., M.S., and Ph.D. degrees in control theory and control engineering from Chongqing University, Chongqing, China, in 2006, 2008, and 2010, respectively.

From 2018 to 2019, he was an Academic Visitor with the University of Auckland, Auckland, New Zealand. He is currently a Professor with the School of Electrical Engineering, China University of Mining and Technology, Xuzhou, China. His research interests include wireless power transfer and intelligent control.

Hongtai Zhang received the B.S. degree in electrical engineering in 2020 from China University of Mining and Technology, Xuzhou, China, where he is currently working toward the M.S. degree with the School of Electrical Engineering.

His research interest includes wireless power transfer.

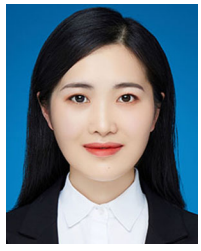

Nan Wei received the B.S. degree in electrical engineering from Yancheng Institute of Technology, Yancheng, China, in 2019. She is currently working toward the M.S. degree with the School of Electrical Engineering, China University of Mining and Technology, Xuzhou, China.

Her research interest includes wireless power transfer.

Shuze Zhao received the B.S. degree in electrical engineering in 2018 from China University of Mining and Technology, Xuzhou, China, where he is currently working toward the Ph.D. degree with the School of Electrical Engineering.

His research interest includes wireless power transfer.

Jiaan Yan received the B.S. degree in electrical engineering in 2021 from China University of Mining and Technology, Xuzhou, China, where he is currently working toward the M.S. degree with the School of Electrical Engineering.

His research interest includes wireless power transfer.

Xiangyu Song received the B.S. degree in electrical engineering in 2019 from China University of Mining and Technology, Xuzhou, China, where he is currently working toward the M.S. degree with the School of Electrical Engineering.

His research interest includes wireless power transfer.

Lijuan Xiang was born in Chongqing, China, in 1989. She received the B.S. degree in automation and the Ph.D. degree in control theory and control engineering from Chongqing University, Chongqing, China, in 2012 and 2017, respectively.

From 2016 to 2017, she was a joint Ph.D. candidate with the Department of Electrical Engineering, The Pennsylvania State University, State College, PA, USA. From 2018 to 2020, she did Postdoc with the College of Physics and Optoelectronic Engineering, Shenzhen University, Shenzhen, China. In 2020, she joined the School of Automotive and Transportation Engineering, Shenzhen Polytechnic, Shenzhen, China, where she is currently a Lecturer. Her research interests include power electronics, wireless power transfer, and electric vehicles.

Zhijuan Liao received the B.E. and Ph.D. degrees from the College of Automation, Chongqing University, Chongqing, China, in 2014 and 2019, respectively.

She is currently a Lecturer with the School of Electrical Engineering, China University of Mining and Technology, Xuzhou, China. Her research interests include wireless power transfer and power electronics.